

AN ABSTRACT OF THE THESIS OF

Robert Kimmell for the degree of Master of Science in Chemical Engineering
presented on September 24, 2009.

Title: Synthesis and Characterization of Magnetic Composite Materials

Abstract approved: _____

Alex Yokochi

Iron epoxy composite materials were made and their relative magnetic permeability was measured. A measurement device was created to measure the relative magnetic permeability for the specific application. This device proved to be accurate and reliable. The magnetic properties of composite materials have been shown to be controllable, with a linear response to volume fraction of iron in the composite. A material with a maximum relative magnetic permeability was achieved at $\mu_r = 650$. Curing the composite material in a magnetic field proved to increase the relative magnetic permeability of the composite when the axis that the composite was aligned was the same as the direction that the measurement device reads. The perpendicular direction produced no change in relative magnetic permeability.

Nanocomposite magnetic materials were investigated based on the use of superparamagnetic nanoparticles. The iron nanoparticles were produced in both

a batch reactor and a microfluidic system. The microfluidic system consisted of a micromixer provided by NanoBits, Inc. and a length of PEEK tubing. A half factorial experiment was performed on the microfluidic system to determine the important factors when controlling the size of iron nanoparticles. The nanoparticles were measured for crystal size by x-ray diffraction using Rietveld refinement to model the size strain broadening caused by the small crystal size. Rietveld analysis was performed with the help of the software package FullProf.

©Copyright by Robert Kimmell
September 24, 2009
All Rights Reserved

Synthesis and Characterization of Magnetic Composite Materials

by

Robert Kimmell

A THESIS

submitted to

Oregon State University

in partial fulfillment of
the requirements for the
degree of

Master of Science

Presented September 24, 2009

Commencement June 2010

Master of Science thesis of Robert Kimmell presented on September 24, 2009.

APPROVED:

Major Professor, representing Chemical Engineering

Head of the School of Chemical, Biological and Environmental Engineering

Dean of the Graduate School

I understand that my thesis will become part of the permanent collection of Oregon State University libraries. My signature below authorizes release of my thesis to any reader upon request.

Robert Kimmell, Author

TABLE OF CONTENTS

	<u>Page</u>
1 Introduction	1
2 Macro Composite Materials	4
2.1 Problem Statement	4
2.2 Experimental	4
2.2.1 Summary of Experiments	6
2.3 Analysis and Discussion	10
3 Nano Composite Materials	14
3.1 Introduction	14
3.1.1 Problem Statement	14
3.1.2 Properties of Nanoparticles	14
3.1.3 Nanoparticle Synthesis	17
3.1.4 Micro Mixers	19
3.1.5 X-Ray Diffraction	20
3.1.6 Design of Experiments	25
3.2 Experimental	28
3.2.1 Synthesis of Nanoparticles	28
3.2.2 Batch Reactor Nanoparticle Synthesis	29
3.2.3 Micromixer Nanoparticle Synthesis	30
3.2.4 Summary of Experiments	32
3.3 Results	32
3.3.1 Post synthesis nanoparticle processing	32
3.3.2 Synthesis in Micro Channel System	33
3.4 Analysis and Discussion	36
3.4.1 Particle Size Determination via X-ray Diffraction	36
3.4.2 Synthesis of Nano Particles via Micromixer	39
3.4.3 SEM Analysis	42
4 Conclusions and Recommendations	48
Bibliography	51

LIST OF FIGURES

<u>Figure</u>		<u>Page</u>
1.1	Magnetic Hysteresis Loop	2
1.2	Magnetic Permeability	3
2.1	Magnetic Permeability Measurement Device Illustration	7
2.2	Magnetic Permeability Measurement Device	8
2.3	Aligned Macro-magnetic Composite Mold	9
2.4	Macrocomposite measurement device reliability study.	11
2.5	Macrocomposite measurement device reliability study with regression analysis.	12
2.6	Aligned Macrocomposite Analysis	13
3.1	Magnetic Alignment: <i>The two different configurations for a magnetic material.</i>	16
3.2	Nanoparticle Synthesis Batch Reactor	31
3.3	Nanoparticle Synthesis Micromixer Configuration	31
3.4	Micro Reactor Nanoparticle Phase ID	34
3.5	Rigaku Rapid X-Ray Diffraction Instrument	37
3.6	SEM image of Iron nano particles at 3000x magnification.	44
3.7	SEM image of Iron nano particles at 12,000x magnification.	45
3.8	SEM image of Iron nano particles at 50,000x magnification.	46
3.9	SEM image of Iron nano particles at 200,000x magnification.	47

LIST OF TABLES

<u>Table</u>		<u>Page</u>
2.1	Macro Composite Experiment 1	7
2.2	Macro Composite Experiment 2	8
3.1	Raw Material List.	28
3.2	Design of Experiment 1	32
3.3	Design of Experiment 2	33
3.4	Design of Experiment 1 Data	35
3.5	Design of Experiment 2 Data	35
3.6	Synthesis of Nano Particles via Micromixer Design of Experiment 1 Analysis of Varriance.	40
3.7	Synthesis of Nano Particles via Micromixer Design of Experiment 2 Analysis of Varriance.	41

1. Introduction

The miniaturization of technology is always a driving force for innovation. One of the current bottlenecks to miniaturizing communication devices are inductors, specifically high frequency inductors. High frequency inductors are used in communication devices such as WiFi radios. The production high performance micro inductors could lead to single chip communication devices allowing smaller systems.

Inductors perform poorly at higher operating frequencies due to Ferromagnetic Resonance (FMR). A stiff magnetic material will hold energy for a short time after the external source has been removed. When the time the magnetic field takes to relax is similar to the time between cycles, the inductor no longer serves its purpose. A very soft magnetic material will not hold this energy as long and therefore can operate at higher operating frequencies. One way this soft magnetic material can be produced is by using nanosized magnetic particles. If the particles are below a critical diameter, a superparamagnetic material can be formed. Superparamagnetism occurs when the magnetization energy is similar to the thermal energy. This causes the particles to only be magnetized when an external field is present.

The classification of a magnetic material as hard or soft is used to distinguish ferromagnetic materials based on their coercivity. A magnetic material can be shown to be hard or soft by experimental measurements, specifically a magnetic hysteresis loop. A magnetic hysteresis loop is a plot of the field strength (H)

versus the resulting flux density (B) of the magnetic material as seen in Figure 1.1. A material with a low coercivity is a soft magnetic material while a material with high coercivity is a hard magnetic material. Magnetic saturation and relative permeability are two other important properties of magnetics in inductors. These values are displayed on a B versus H plot, at the initial magnetization of the material, as shown by Figure 1.2. For the application of a high frequency inductor, coercivity is minimized while the magnetic permeability is maximized for optimum performance.

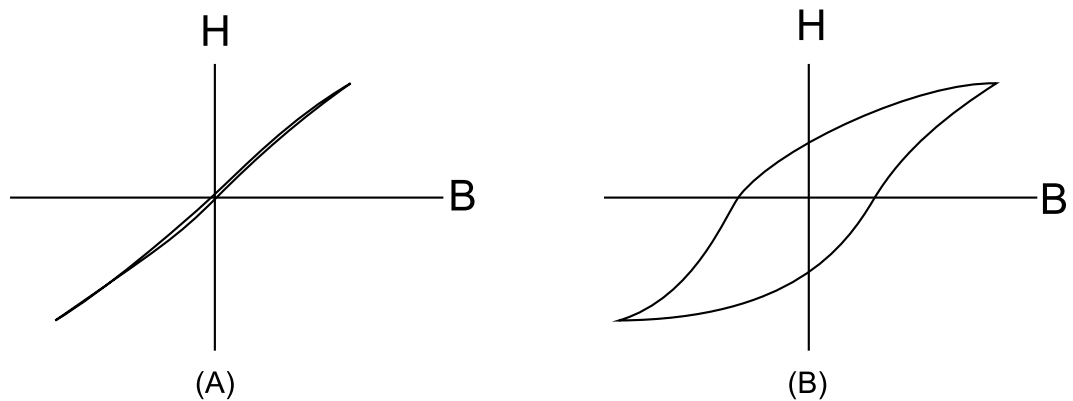


Figure 1.1: Magnetic Hysteresis Loop: (A) Example of a soft magnetic material. (B) Example of a Hard magnetic Material.

Two applications of magnetic materials will be discussed in this work. The first is an application of a macro composite material for use in a OSU wave energy effort. The second application discussed is the initial development of nano composite materials for use in high frequency inductors (multiple Ghz).

Magnetic nano particles that are sufficiently small can be used as a soft magnetic material for use in high frequency inductors. The production of iron nanopar-

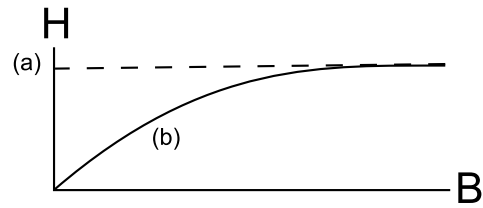


Figure 1.2: Magnetic Permeability: (a) Point of magnetic saturation. Slope of curve at (b) is the relative magnetic permeability.

ticles of the required size has been shown in literature, for example these particles are synthesized in a batch process with a size as low as 6 nm.[1] The ability to control the exact size and distribution of these particles is greatly desired, so that the performance of the device can be optimized.

The relative permeability of a material, $\mu_r = \frac{\mu}{\mu_o}$ is a dimensionless quantity and therefore no units will be presented in this work.

2. Macro Composite Materials

2.1 Problem Statement

Sustainable methods to produce electricity are in high demand. One solution to fill this need is to harness the energy in ocean waves by a linear motion generator. This linear generator uses magnetic induction to produce electricity. For the system to achieve maximum efficiency, the magnetic losses in the system have to be minimized. A material with a tunable magnetic permeability will allow the optimization of the flow of magnetic energy. As with all sustainable energy products, the material must be low cost to keep the new technology competitive against traditional energy generation methods. The magnetic material is required to be lightweight, have a relative magnetic permeability of 500, and made out of an inexpensive material.

2.2 Experimental

Initial experiments on magnetic composite materials began with macro sized particles rather than nano sized particles. This was done for practical reasons as macroparticles are inexpensive and easily obtained. The objective of these experiments is to determine the magnetic properties of composite materials. Iron powder (200 mesh, VWR) was mixed with West Systems epoxy at various concentrations to determine the relative magnetic permeability of the resulting materials. The composite material was also cured under a magnetic field. This was done to de-

termine to what extent the magnetic permeability of the composite material was dependent of the micro structure of particles caused by magnetic alignment.

Two experiments were performed using the macro iron particles. The first experiment was designed to test the response of the measurement device. A lab made measurement device, which consists of a hand wound solenoid, magnet, and power supply, was created to make a inexpensive method to test the effective magnetic permeability of the samples, which can be seen in Figure 2.1. This test device works by placing the sample in the center of a coil. The sample acts as the magnetic core of a solenoid. When the coil is energized, a magnetic field that flows through the sample is created that exerts a force on a magnet below the device. A force balance can be performed using Equation 2.1, where F is the force, μ_r is the relative magnetic permeability, μ_0 is the permeability of space, N is the number of turns in the coil, I is the current applied to the coil, A is the cross sectional area of the sample, and L is the length of the coil.

$$F = \frac{\mu_r^2 \mu_0 N^2 I^2 A}{2L^2} = mg \quad (2.1)$$

The variables that change from test to test are μ_r and I . Equation 2.1 can be reduced down to Equation 2.2, where C is a constant. The constant C can be solved by employing a reference material with a known magnetic permeability, in this case mild steel was used, which has a μ_r of about 5000.

$$\mu_r = \frac{C}{I} \quad (2.2)$$

The accuracy is not as important as the precision in this device, as this set of experiments was used to qualitatively examine the properties of the nanocomposite material. Selected amounts of Iron powder (200 mesh, VWR) were added to 1.6 fl.oz. of West Systems Epoxy, and well mixed. This mixture was then poured into a mold, and placed in vacuum chamber. The samples were cured under vacuum to reduce air voids created while mixing. Once cured, the samples were cut into thinner strips which would fit into the measurement device. Replicates of this experiment were collected to examine the precision of the testing device, while different volume fractions were collected to determine if the measurement device was responsive enough for our needs.

The second experiment performed in this section was to determine the effects of curing composite materials in a magnetic field. Samples were prepared as in the previous experiment. However, while curing, a magnetic field was placed across the mold, either in the long direction, or the short direction of the mold illustrated in Figure 2.3.

2.2.1 Summary of Experiments

Experiments performed using Iron powder mixed with epoxy are summarized in Table 2.1. Experiments to test the effects of curing samples under a magnetic field are summarized in Table 2.2.

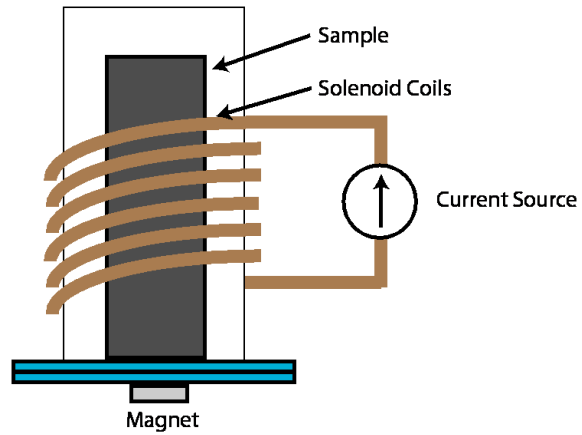


Figure 2.1: Magnetic Permeability Measurement Device Illustration: Sample is placed in the center of the solenoid coil, the current is modified so that the resulting magnetic field is in balance with a magnet in the bottom of the device being pulled by gravity. When the forces of equal, the magnetic permeability of the sample can be extracted.

Table 2.1: Macro Composite Experiment 1: Initial experiment to determine the effects of particle loading on the magnetic properties.

Run Number	Volume Percent Iron
1	1.64
2	3.61
3	7.47
4	13.04
5	18.36
6	25.92
7	31.03
8	37.49

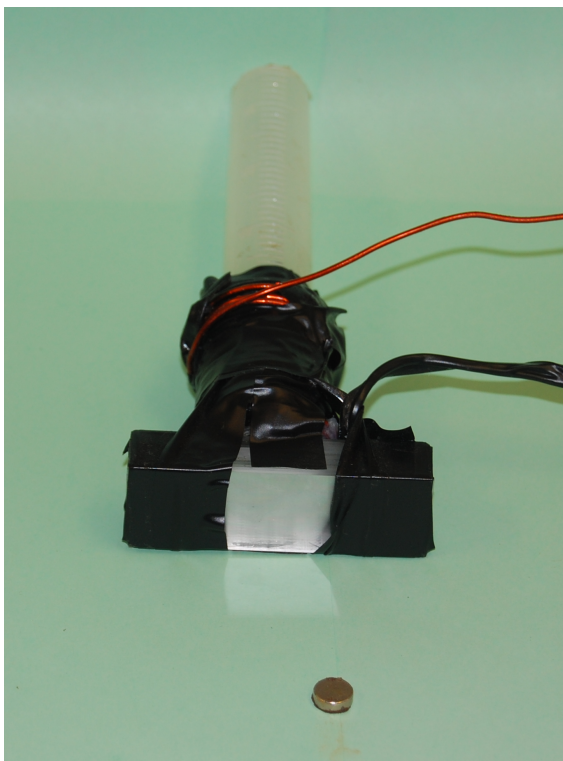


Figure 2.2: Magnetic Permeability Measurement Device

Table 2.2: Macro Composite Experiment 2: Experiment to determining the effect of curing in a magnetic field.

Run Number	Volume Percent Iron
1	3.60
2	18.00
3	31.00



Figure 2.3: Aligned Macro-magnetic Composite Mold

2.3 Analysis and Discussion

To test the effects of magnetic alignment of the macro composite material, the measurement device must be benchmarked for accuracy and reliability. Several experiments were performed where the volume percent of iron in the composite material was varied from 1.64 percent to 37.5 percent. Each sample was replicated three times to determine the precision of the data. The results of this experiment can be seen in Figure 2.4. The last set of data points on this figure is statistically different from the rest of the data. This point is removed in Figure 2.5, where a regression analysis is performed. The samples that yielded this datum were examined and it was noticed that they had many air voids within the composite, likely due to the fact that the viscosity of the uncured composite was too high for the vacuum chamber to effectively remove all of the air from the sample. A higher concentration of air voids in the composite would lower the relative permeability.

The next step in the experiment was to examine the effects of curing the composite material under the presence of a magnetic field. The experiment was performed at three volume fractions, with a fully randomized run order. Two different directions of alignment were tested as well as an unaligned sample. As seen in Figure 2.6, the widthwise and unaligned samples are indistinguishable, while the lengthwise sample had a statistically higher relative permeability. It was concluded rearranging the magnetic particles through the use of an external magnetic field at the time of curing can significantly enhance the magnetic permeability of the composite material.

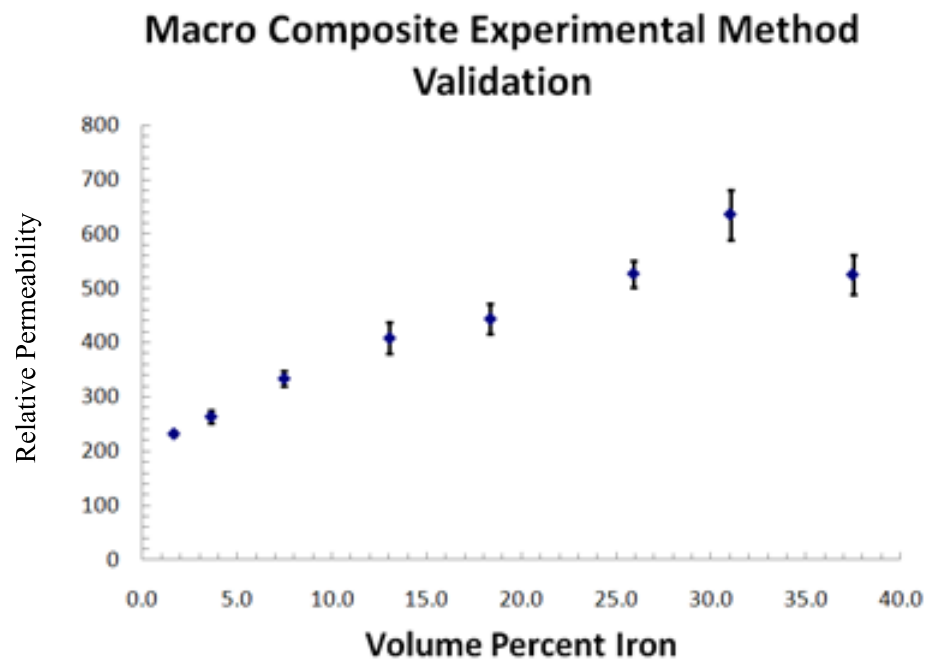


Figure 2.4: Macrocomposite measurement device reliability study.

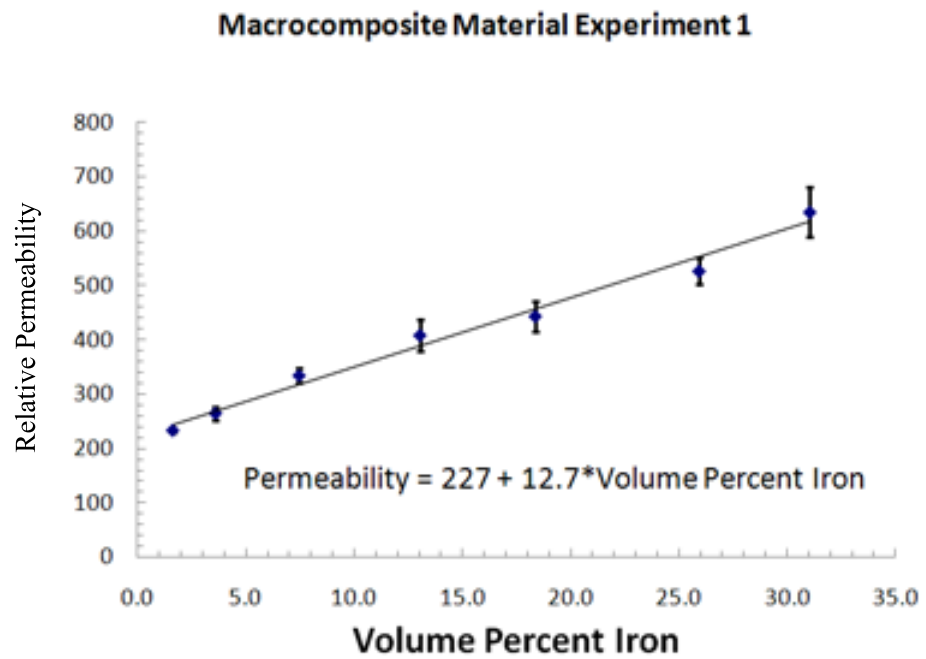


Figure 2.5: Macrocomposite measurement device reliability study with regression analysis.

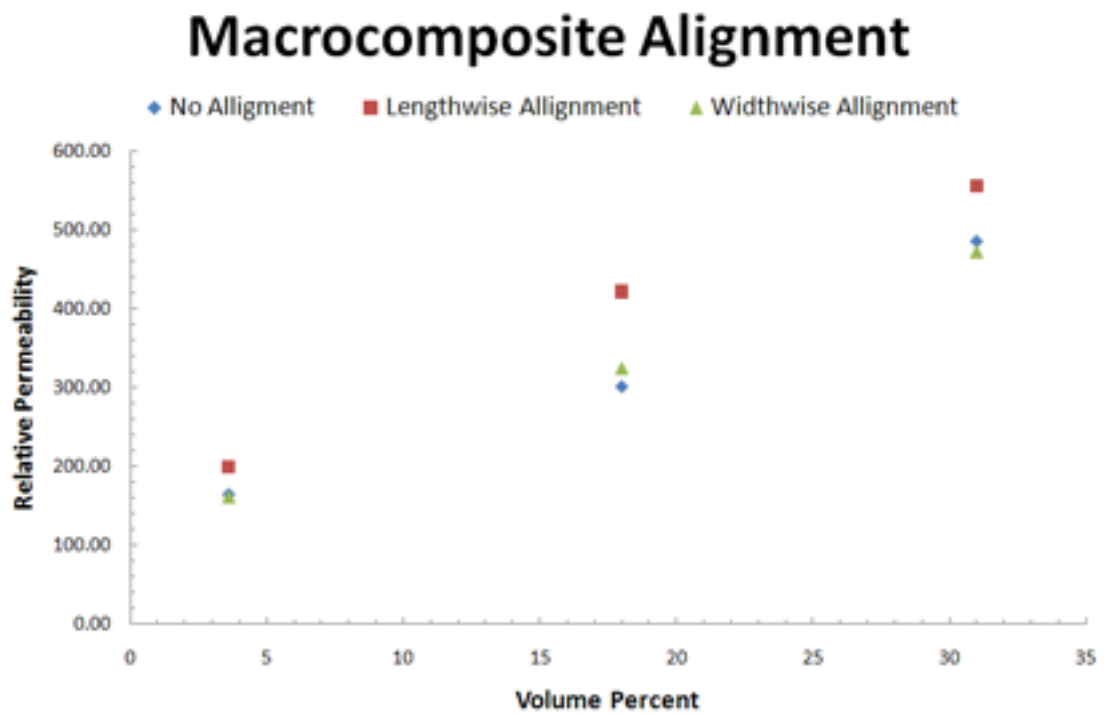


Figure 2.6: Aligned Macrocomposite: Samples cured under magnetic field passing through the long direction (lengthwise) had a significant effect on the relative permeability, while alignment along the short axis (widthwise) did not have an effect.

3. Nano Composite Materials

3.1 Introduction

3.1.1 Problem Statement

A second class of magnetic materials examined is nanocomposite materials to support the endeavour of high frequency inductors. For this purpose, a method to produce uniform magnetic nanoparticles with a controllable size in which the size is below the superparamagnetic limit, which for most materials is about 20 nm, needs to be developed. The use of a micromixer to produce these nanoparticles is therefore examined here.

3.1.2 Properties of Nanoparticles

Nanoparticles can have significantly different properties from their macro particle counterparts. A nano material can be defined as a material which is made of building blocks that have at least one dimension less than 100 nm. These materials can show enhanced properties that are affected by the small size. The shape and size that nanomaterials can take varies from three dimensional particles, to one dimensional materials such as carbon nano tubes to two dimensional sheets to zero dimensional such as quantum dots. A simple example of a property affected is the ratio of surface area to volume. The surface area to volume ratio, $R = \frac{6}{D}$ where R is the ratio and D is the diameter, is 600 for a 1 mm particle, while it

is 600,000,000 for a 100 nm particle. Some of the properties that may change are index of refraction, melting point, and heat capacity.

The magnetic properties of a material can be classified by their response to an external magnetic field in three categories; diamagnetic, paramagnetic, and ferromagnetic. A diamagnetic material is a material which does not become magnetized when an external field is applied. Diamagnetic properties come from the orbital motion of electrons in the atoms of the material. Small electrical currents create magnetic fields. A paramagnetic material will become magnetized only when an external field is applied. With no external field present, the paramagnetic domains will be randomly aligned. However, when an external field is applied, the domains will all orient in the same direction as the field. A ferromagnetic material's magnetic dipoles are coupled causing long-range order, and the material can remain magnetized even in the absence of an external magnetic field. The areas of long-range order, known as magnetic domains, are generally smaller than the grain size. [2] The configurations of paramagnetic and ferromagnetic materials can be seen in Figure 3.1.

The property that is important to this discussion is the magnetic relaxation time. Paramagnetic materials, at a temperature greater than 0 K, behave non-ideally. When the externally applied magnetic field is removed from the material, it will not return to its normal state instantly, there is a delay τ , where τ is the relaxation time of the induced magnetic energy. Where the operating frequency ($f = 1/t$) of a device is in the same order of magnitude of τ , the material will display a large magnetic hysteresis loop which will reduce the device performance.

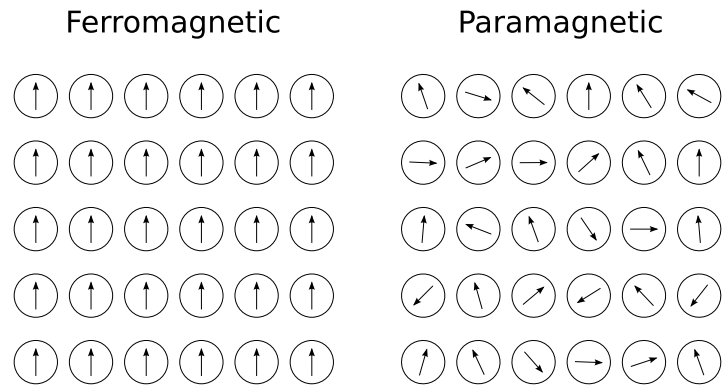


Figure 3.1: Magnetic Alignment: *The two different configurations for a magnetic material.*

A nanomaterial behaves differently in this situation since τ is dependent on crystal size, the small crystal will relax faster, as seen in Equation 3.1.[3]

$$\tau^{-1} = f_0 \exp(-KV/kT) \quad (3.1)$$

where K is the anisotropy constant, V is the crystal volume, k is the Boltzmann constant, T is the temperature and f_0 is a frequency factor of the order of 10^9 sec^{-1} . A material will behave paramagnetically if $\tau/t \leq 1$. Therefore the upper limit of the paramagnetic region can be reduced to Equation 3.2.

$$V_p = 25kT / K \quad (3.2)$$

where V_p is the size limit of superparamagnetic behavior.

3.1.3 Nanoparticle Synthesis

There are two primary methods to produce nanoparticles, the "top-down" and the "bottom-up" approach. These two use inherently different principles to create nanoparticles. The "top-down" approach resides around transforming a bulk material into nano-sized particles. This is the least common approach, as it is the least flexible, is generally not suited for synthesizing uniformly shaped particles, or very small particles [4]. The most common top-down synthesis method relies on force to break a bulk material down. This can be accomplished by mechanical crushing, pulverization and arc discharge. The materials that are processed in this manner are generally large in size with a very wide size distribution [5].

Bottom-up approaches are much more common and have the ability to create all ranges of sizes and shapes of nanomaterials. A "bottom-up" approach can be as simple as reducing metallic ions to as complex as laser pyrolysis. The processing of materials into nanomaterials can be done by a physical or chemical route. Physical methods that have been used to create nanoparticles in the "bottom-up" method include vapor condensation, spray pyrolysis, thermochemical decomposition of metal-organic precursors by flame reactor, high temperature aerosolization [6]. Chemical synthesis methods can be carried out by reducing metal ions with chemical reducing agents such as hydrazine[7], NaBH_4 [1], etc. These methods are also combined with dispersing agents to decrease the size variability.

One more classification of the different methods to produce metallic nanoparticles is the medium in which the reaction is performed. Vapour phase synthesis

methods include chemical vapour deposition, laser pyrolysis, and arc discharge. Liquid phase synthesis methods include sol-gel processing, micro-emulsions, and hydrothermal techniques. The primary solid synthesis method is ball milling. CVC processes involve evaporating a metal target, which undergoes a vapour phase chemical reaction, and later condensed to form nanoparticles [8]. This method has been shown to be able to produce loosely agglomerated nano-sized silicon nitride particles in large quantities [9].

An alternative gas phase synthesis method is arc discharge. This is the common methods for synthesizing nanocapsules. Ni encapsulated in graphite shell was successfully synthesized by a modified arc discharge method [10]. The arc discharge method involves metal precursors embedded in a graphite electrode, which undergoes arc vaporization. Carbon nanotubes have also been synthesized in this manner with processes ranging from simple single wall CNT's to whisker like multi-wall CNT fibers [11, 12].

The primary liquid processing method is implementing a microemulsion. There are three important components in this system, two are nonmiscible solvents, and the third is a surfactant. The surfactant will create microdroplets in the system that seed particle formation. This method has been used to produce Iron and Iron Oxide nanoparticles [13]. Nanoparticles can also be produced by hydrothermal processes. In this case, aqueous solutions, vapors, and fluids react with a solid material. High pressure and temperature cause soluble organic materials to form nanocrystals[14]. Chemical reduction of metallic ions is similar to the microemulsion synthesis method. A surfactant is utilized to both prevent agglomeration and

to control the nucleation and growth mechanisms. The particle growth occurs in two steps, nucleation and growth. The reaction kinetics of the first step, nucleation, is slow; while the second step, growth, is much faster. To increase particle size distribution and decrease particle size, palladium ions can be introduced into the system to act as nucleation sites[1].

For the present work, nanoparticles that are both small and size controlled are required. The method of metallic ion reduction was chosen for this work, specifically reduction by NaBH_4 . Both iron and nickel nanoparticles have been shown to be synthesized in this method with a controllable size and size distribution [15, 1]. This method also has the advantage of requiring little specialized equipment or materials, which meets a requirement of a cost efficient process. This process is capable of being run in a micromixer, which is one of the goals of the project.

3.1.4 Micro Mixers

There are multiple ways to increase the uniformity of particle size distributions when synthesizing nano sized particles. The particle size and size distribution can be changed by varying the reaction conditions.[16] Micromixers have shown to increase the the contact time between two fluids which leads to faster mixing. It is theorized in that a micromixer will be able to produce nano particles with very narrow particle size distribution.

Micromixers operate in two basic principles, active and passive. An active micromixer uses an external energy source to aid in the mixing of two or more

fluids. These external energies can include ultrasound, acoustic vibrations, periodic fluid pumping, small impellers and vibrating membranes. [17]

A passive micromixer relies on bringing the fluids closer thus decreasing the path length for molecular diffusion needed to achieve mixing. This is primarily done by splitting the flow into smaller channels, then interweaving the fluids creating very thin layers. Parallel laminated micromixers are the simplest configuration. Each fluid starts with its own stream, which are all joined together creating a laminar flow with very long contact time. [18]

Previous studies on nanoparticle synthesis have focused on premixed reactants which are reacted in a capillary tube. [19]

3.1.5 X-Ray Diffraction

The primary analytical tool used in this work is x-ray diffraction. X-ray diffraction is a better size analysis tool in this case because it directly measures the size of crystal domains in the sample. Optical size measurements determine the physical size of a particle that may be made of several clusters of crystals. This is important because the magnetic relaxation time for a material is determined by the crystal size, not the particle size.

X-ray diffraction is a very effective tool for quantitative analysis. It has the ability of to determine the the atomic structure of crystals. X-ray diffraction benefits over other radiation measurement methods as it can reveal the structure of matter down to 10^{-10} m.

The first step to X-ray diffraction is creating X-rays. There are many characteristics of X-rays that need to be controlled. An X-ray is an electromagnetic radiation source just like light. However, visible light has a wavelength on the order of 6000 \AA , X-ray radiation ranges from $0.5 - 2.5 \text{ \AA}$. An x-ray is produced when a particle, such as an electron, is charged with enough kinetic energy is slowed rapidly. The kinetic energy released by the deceleration of the particle is transferred in the form of heat and x-rays. An electron is usually the particle of choice because it is easy to produce.

The spectrum which is emitted from an x-ray tube is continuous. The lowest wavelength of x-ray is known as the short-wavelength limit (λ_{SWL}). The intensity of x-rays increases from this point and peaks, then gradually rolls off to zero. The intensity of radiation is proportional to the voltage in the source. This continuous nature of the radiation spectrum is due to the random nature of the decelerating electrons. The short-wavelength limit is caused by the fact that an electron has a specific initial velocity required to produce an electron before it is decelerated. This is also why there is no finite upper limit to the x-ray spectrum.

Once the voltage on the x-ray source is raised to a high enough energy, the spectrum is no longer continuous. Narrow, higher intensity peaks that are characteristic of the anode target overlay on the continuous spectrum. In the case of a Copper radiation source, there are several groups of peaks that form. These lines are indicated by subscript Greek letters such as $K_{\alpha,1}$, $K_{\alpha,2}$ and $K_{\beta,1}$. The K_{α} set are generally close together and are only visible as separate peaks at very high 2θ values.

Once these x-rays are produced, we can do something useful with them, examine a sample. The x-rays are sent through a collimator which produces x-rays which are oriented in a beam. The degree of alignment depends on the size of the collimator, where a smaller collimator will produce weaker flux of x-rays. The x-rays are then pointed into the sample where the diffraction takes place. Diffraction occurs when an x-ray is scattered by the electrons in an atom. This diffraction is not universal, it will only occur when certain geometric conditions are present. These geometrical conditions are described by the Bragg equation.

$$n\lambda = 2d\sin\theta \tag{3.3}$$

The Bragg equation states that diffraction can only occur when the incident beam makes the defined angle to the crystal surface, for the diffracted beam to be produced. For a single crystal experiment, it is very important to understand this concept, as the sample must be placed in the diffractometer in a way that these conditions can be met. If the crystal is in the correct position, there will not be a diffracted beam. In a powder experiment, the distribution of crystal orientations should be randomized, which leads to there always being a portion of the sample that is correctly aligned.

In a perfect system, an infinite number of crystal planes, the diffracted beam will be extremely narrow. The reality is that the diffracted beam has shape. This shape is introduced by both the instrument and constructive / deconstructive interference nature of the wave function that describes the x-rays. This shape

broadens as the number of crystal layers decreases. It is this fact that can be used to determine the size of crystal domains by the use of x-ray diffraction.

To accurately determine what the source of the peak broadening, the entire profile needs to be analyzed. The Rietveld Method[20], also known as Whole Powder Pattern Fitting or WPPF, performs this task by fitting various functions by a least squares measurement. The result of the analysis is a set of characteristic parameters that define instrument and crystal structure. This process is implemented by the software package FullProf [21] which can be used to extract the average crystal size a sample.

In Rietveld fitting, the first step is to model the background. In most cases, this can be modelled by a simple polynomial with three to five coefficients. Most samples will have an easy to deal with background, however, when working with Iron the background can be difficult. Iron will introduce a fluorescence background when using a Copper based x-ray source, which adds to the other background sources such as air scatter. The amount of fluorescence background will change with the amount of Iron in the sample, which will vary from experiment to experiment [22].

The peaks that are fit using the Rietveld method are also difficult. They are not purely Gaussian, they also have a Lorentzian contribution to the peak shape. To handle this, Tomandl (1987) proposed that the following function be used:

$$T(2\theta) = \eta L(X, Y, \chi) + (1 - \eta)G(u, v, w, \chi) \quad (3.4)$$

where $L(x)$ is the Lorentzian function, $G(x)$ is the Gaussian function, $x =$

$(2\theta - 2\theta_{peak})/\Gamma$, 2θ is the peak position, Γ is the full width at half maximum, and η is the mixing factor [23]. In these function there is a set of parameters that are refined to fit the instrumental contribution to peak shape, known as Caglioti parameters (UVWXY)[24]. These parameters will be refined for a standard material so that the instrumental contribution to peak broadening can be eliminated.

The main source of broadening that we are concerned with is due to small crystal size. A crystallite with a size bellow $1 \mu m$ will have have an integral breadth β which will follow the Sherrer (1918) equation:

$$\beta = \frac{\lambda}{\tau \cos\theta} \quad (3.5)$$

where τ is the crystallite size.

When performing profile fitting there are many variables that must be accounted for. Each diffraction instrument will produce different experimental errors that must be accounted for. The distance from the source to the sample, the sample to the detector, misalignment of the sample and detector will all produce shifts in the data. Using a material, which is made of large crystals (on the order of $10\mu m$), which has been annealed to remove all stress, can be used as a standard to measure these error.[25] The standard diffraction profile is taken under the same conditions in which the experiments are going to be performed. All instrumental errors such as peak shifts and peak shape functions are fitted. Once these parameters are determined, the fir to a profile produced by a sample with unknown size can be refined and the unknown size can be extracted from the fit parameters. It

is assumed that the instrumental error will be constant, therefore the only source of peak broadening is due to size broadening. It has been shown in literature that this method for measuring crystal size is accurate down to 1 nm in a study that directly compared the size of cerium oxide nanoparticles via TEM and Rietveld refinement[26].

3.1.6 Design of Experiments

When performing an experiment that has a large number of variables, the number of tests that needs needs to be performed in order to examine the effects of the variables and their interactions when changing one factor at a time is enormous. The sheer number of tests required can be cost and time prohibitive, and in some cases, impossible. For example, in a system where two factors at two levels are considered, complete characterization will require 6 experiments. More efficient methods to perform this work using statistics exist. When statistics is applied to experimental procedure, it is known as Design of Experiments[27]. The fundamental concept is that an experiment needs to be designed correctly, before the experiment is executed, in order to have data that is meaningful.

The terminology used in the DOE is different that in other areas. A factor describes a variable in an experiment, such as temperature, and is referred to as x_i where i is the number assigned to the factor. Nuisance factors, which are uncontrolled variables such as weather, day, measurement error, are denoted as z_i where i is the number associated with that nuisance factor. The output of the

experiment, or the measurement, such as product yield, is denoted as y_i .

The overlying concept around DOE is the random distribution, more specifically the normal distribution.

$$z = \frac{y - \mu}{\sigma} \quad (3.6)$$

where μ is the mean, y is the random variable and σ is the standard deviation. A special case which is called the Standard Normal Distribution is when $\mu = 0$ and $\sigma^2 = 1$. The importance of the random distribution relies in determining if an experimental result occurs from pure chance, meaning that the controlled variables could have been anything and the same result would have happened, or the results came from the influence of the factors. To check this a t-test is performed. A t-test assumes that the samples are drawn from independent populations that can be assumed to follow the normal distribution. The actual statistical value of the t-test changes with experimental setup and is tabulated in many statistical books[28].

The simplest experiment, one factor with one level and one response, will not benefit from a design of experiment procedure. There is only one possible way to arrange the order of experiments, as there is only one run with the experiment. If the experiment would be run with the single factor having two levels, the order at which these factors are tested can have an influence on the outcome. Outside variables including pure variability, weather, instrument error and human error can influence each trial differently. The importance of randomizing becomes even more clear when the number of levels is increased. For example, a single factor

with four levels is investigated. Traditional thought might assume that each level would be run in order from lowest to highest. The goal of this experiment is to determine if the level has an effect on the outcome. At the end of the experiment, examining at the data it shows that the output increased with the level increasing. However, there are two components in this measurement, the real contribution of the factor, and the contribution due to error. Since all levels were run in order, there is no possible way to determine if the error or the factor was producing the results. If this experiment were to be completely randomized, the output would only be influenced by the factors contribution.

When starting a large experiment with multiple factors which little are known about, a screening design of experiment is important to run. This not only helps the investigator understand the system better, but also allows factors to be eliminated from future studies if it is deemed unimportant. The most common type of screening factor design is the fractional factorial experiment. An experiment that contains three factors, with each factor consisting of two levels, a full factorial experiment would require eight runs. This may be an impractical experiment, however an experiment with four runs would be possible. One half of the factorial experiment can be run without losing critical information. In this case, only the three way interaction would be lost, which in experience is rarely useful information.

3.2 Experimental

The suppliers of the raw materials used in these experiments is summarized in Table 3.2. All materials were used as received.

Table 3.1: Raw Material List.

Material	Supplier
NaBH ₄	Burker
FeCl ₃	Burker
PdCl ₂	Sigma
PolyAcrylic Acid	Sigma

3.2.1 Synthesis of Nanoparticles

Iron nanoparticles were synthesized in batch and micromixer reactors. Batch synthesis was conducted in a 500 mL three neck flask, initially charged with a approximately 0.15 M solution of FeCl₃ underwent vigorous stirring, which is orange in color. The reducing agent, NaBH₄ (3.5 M) was added drop wise. Upon addition of the borohydride solution, a black precipitate formed along with a gas later identified as hydrogen. The reaction was assumed complete when gas evolution ceased. The black precipitate reacted strongly to a magnetic field, which was exploited to wash the particles of byproducts.

To wash the particles, a magnet was placed on the bottom of the flask, which would cause all the particles to migrate towards the magnet. The remaining fluid was then poured off. Clean deionized water was added back into the flask and

the particles were redispersed. This process was repeated several times until the particles appeared pure. The initial method to dry the particles was to leave the container open to the atmosphere, drying overnight. This produced particles that were no longer magnetic. Though the evaporation process, the particles fully oxidized. To solve this problem, the particles were lyophilized at an operating pressure of 200 *m*Torr and an initial temperature of -80°C . This process produced particles that retained the same magnetic properties as the particles dispersed in liquid.

Iron nanoparticles were also produced in a micro chemical system. The goal of producing particles in this method is to decrease the size distribution and have greater control over average particle size. The micro chemical system used consists of a micromixer manufactured by NanoBits. The micromixer is fed by two syringe pumps manufactured by New Era Pump Systems, Inc. Small bore tubing is connected to the exit of the micromixer which ranges in size from 25 microns to 1/16th of an inch. The length of the exit channel varied between experiments. The goal was for the reaction to be complete by the time it exited the channel. The same washing procedure was performed as for the batch experiments.

3.2.2 Batch Reactor Nanoparticle Synthesis

To demonstrate that magnetic metallic nanoparticles can be made, Iron nanoparticles were created in a batch reactor following the procedures described by Huang, K.C. and Ehrman, S.H. [1]. The first set of experiments looked at the production

of Iron nanoparticles using Iron Chloride, Sodium Borohydride, and Poly acrylic acid (PAA). The poly acrylic acid is present for the use as a dispersing agent. A 0.1 M solution of Sodium Borohydride is added dropwise into a 0.01 M solution of Iron Chloride with a Iron to PAA ratio of 1:10, with vigorous stirring, as illustrated in Figure 3.2. This results in the orange iron solution turning black the instant a drop of Borohydride enter the reaction vessel. The reaction is assumed complete when all formation of hydrogen gas has ceased. Further experiments included additions of Palladium Chloride, which was added at a ratio of 1 Palladium ion to 100 Iron ions. In both experiments, the particles produced responded well to a applied magnetic field. They were easily separated from solution by this method.

3.2.3 Micromixer Nanoparticle Synthesis

The configuration of the micromixer can be seen in Figure 3.3. Two syringe pumps sourced from New Era Pump Systems, Inc. pump a mixture of NaBH_4 in one syringe and iron chloride, poly-acrylic acid, and palladium chloride into a micromixer sourced from Nanobits, Inc. The effluent of the micro mixer is sent through a 0.003" ID PEEK tube to increase the residence time for the reaction to complete.

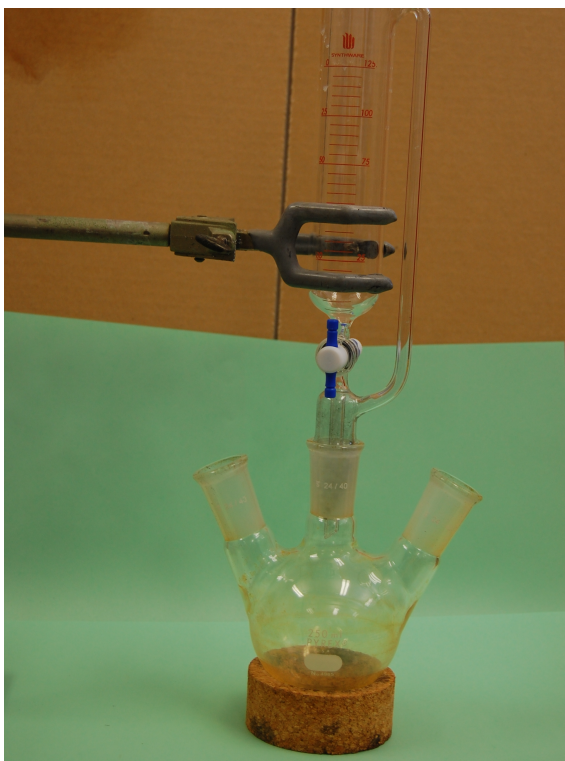


Figure 3.2: Nanoparticle Synthesis Batch Reactor: Configuration of nanoparticle batch reactor.

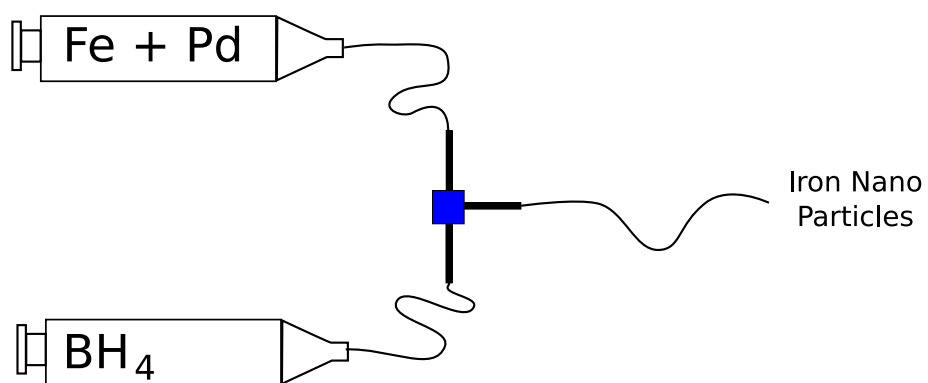


Figure 3.3: Nanoparticle Synthesis Micromixer Configuration

3.2.4 Summary of Experiments

The set-up of the two designs of experiments are summarized in Table 3.2 and Table 3.3 Both experiments were performed by mixing Solution A and Solution B in a micromixer.

Table 3.2: **Design of Experiment 1:** Initial screening experiment to determine important factors. Solution A: 0.81 g FeCl₃ in 40 ml DI Water mixed with 60 mL 3.5% PAA. Solution B: 2.25 g NaBH₄ is added to 50 mL DI Water. 0.1 ml Pd solution (0.01 M) was added when indicated. 0.1 ml 28% ammonia solution was added when indicated. Additions are added to solution A before entering the micromixer.

Run Number	Flow Ratio Fe Sol. : BH ₄ Sol.	Pd Present	pH Modification 2	Size (Å)
1	1:1	Yes	No	28.83
2	2:1	No	No	13.21
3	2:1	Yes	Yes	15.53
4	1:1	No	Yes	13.23

3.3 Results

3.3.1 Post synthesis nanoparticle processing

A batch reactor was used to produce the nanoparticles, that were then washed using a magnet, and left uncovered to dry overnight. The color of the nanoparticles changed from black in solution to an orange powder after drying. An XRD scan showed that the particles were no longer Iron (1). It was concluded that the particles

Table 3.3: Design of Experiment 2: Further screening of important factors. Solution A: 0.81 g FeCl_3 in 50 ml DI Water mixed with 60 mL 3.5% PAA. Solution B: 1 g NaBH_4 is added to 50 mL DI Water. Additions in table are added to solution A before entering the micromixer.

Run Number	pH Modification	Pd Concentration	Reactor Size
	A	B	C
1	1	1	-1
2	-1	-1	-1
3	1	-1	1
4	1	-1	-1
5	-1	1	-1
6	-1	1	1
7	-1	-1	1
8	1	1	1

fully oxidized while air drying, producing Iron Oxide. To solve this problem, lypholyzation was used.

Further experiments were performed, changing the drying method from air drying to lypholyzation. The washed particles, still black in color, were frozen to -80 C. The sample was then placed in the lypholizer running at 200 mTorr. The resulting particles were black in color.

3.3.2 Synthesis in Micro Channel System

The proof of concept has now shows that the methods proposed in (journal articles) are suitable for producing nano particles in a batch reactor. Using the same concentration as in the batch reactor, an experiment using a micro chemical device

for the reactor was performed. The resulting particles were analyzed for Phase ID using XRD. As seen in Figure 3.4, the cell edge is still 2.866 Å.

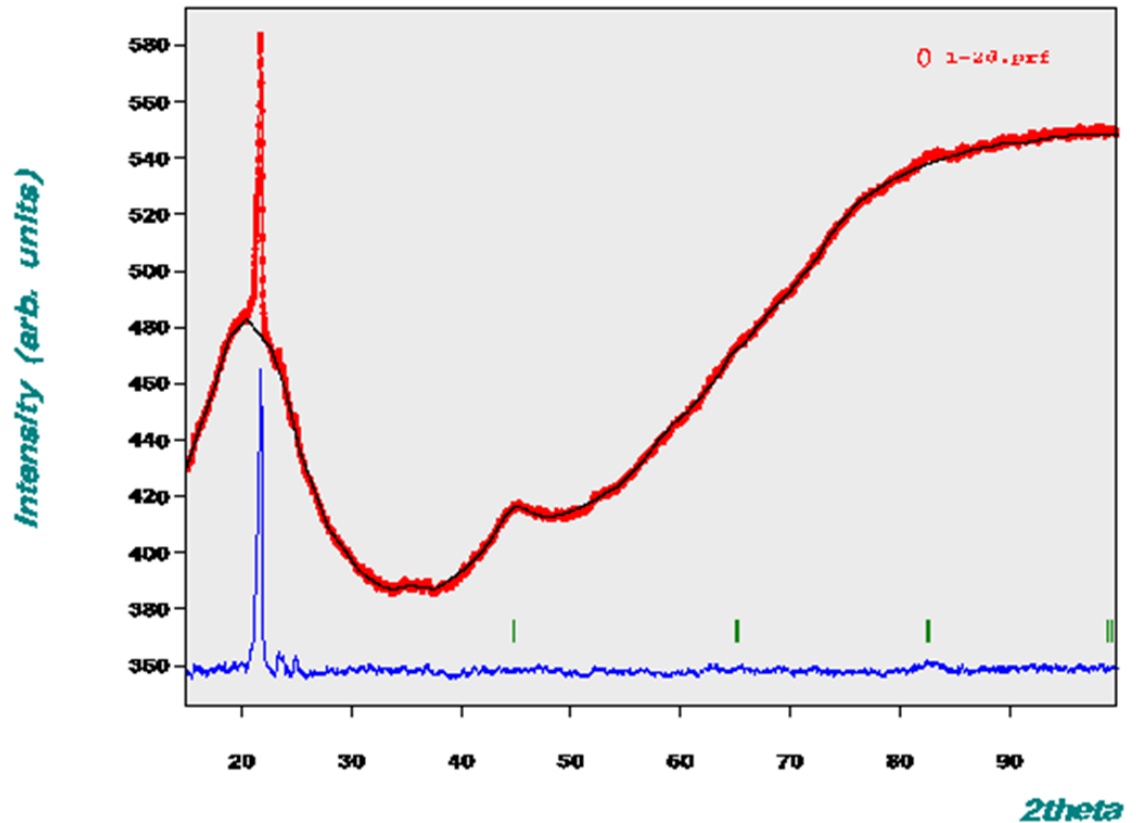


Figure 3.4: XRD Phase ID: XRD scan of Iron Nano Particles produced in a micro reactor with cell edge of 2.866 Å. The vertical lines below the the signal represent the calculated Bragg diffraction location, which match with the peaks. The red line represents the data collected on the sample, the black like is the whole profile fit to a nanocrystalline iron materiel and the blue line is the difference between the observed profile and the calculated profile.

To extend the understanding of this system, an experiment designed to screen the important variables was created. The data of the first DOE found in Table

3.2 can be seen in Table 3.4. A second DOE was performed to narrow the range of parameters so that the response can be assumed linear. The data from this experiment can be seen in Table 3.5.

Table 3.4: Design of Experiment 1 Data

Run Number	Flow Ratio Fe Sol. : BH ₄ Sol.	Pd Present	pH Modification 2	Size (Å)
1	1:1	Yes	No	28.83
2	2:1	No	No	13.21
3	2:1	Yes	Yes	15.53
4	1:1	No	Yes	13.23

Table 3.5: Design of Experiment 2 Data

Run Number	pH Modification	Pd Concentration	Reactor Size	Particle Size (Å)
1	1	1	Small	14.92
2	-1	-1	Small	7.23
3	1	-1	Large	13.03
4	1	-1	Small	11.45
5	-1	1	Small	17.95
6	-1	1	Large	17.61
7	-1	-1	Large	7.66
8	1	1	Large	15.23

3.4 Analysis and Discussion

3.4.1 Particle Size Determination via X-ray Diffraction

Quantitative analysis was performed using the help of x-ray diffraction. Using the principles described previously, the average particle size was determined by peak broadening. Whole profile fitting was performed using the software package Full-Prof, which uses the Rietveld method. A standard, magnesium oxide, which was annealed to reduce internal stress, was used to initially set up the peak broadening due to instrumental factors. The diffraction instrument, Rigaku Rapid, as seen in Figure 3.5, uses a curved 2-D image plate as a detector. If the sample is not perfectly in the center of the cylinder, peak shifts dependent on $\sin\theta$ will occur. The instrumental peak broadening was fit using the Pseudo-Voigt model.

$$H_G^2 = (U + D_{ST}^2)\tan^2\theta + V\tan\theta + W + \frac{I_G}{\cos^2\theta}$$

$$H_L = X\tan\theta + \frac{[Y + F(S_z)]}{\cos\theta}$$

where H_G and H_L are the full-width-half-max values for the Gaussian and Lorentzian functions. U V W X and Y are fitting parameters. The Gaussian function,

$$G(x) = a_G \exp(-b_G x^2)$$

$$a_G = \frac{2}{H} \sqrt{\frac{\ln 2}{\pi}}$$

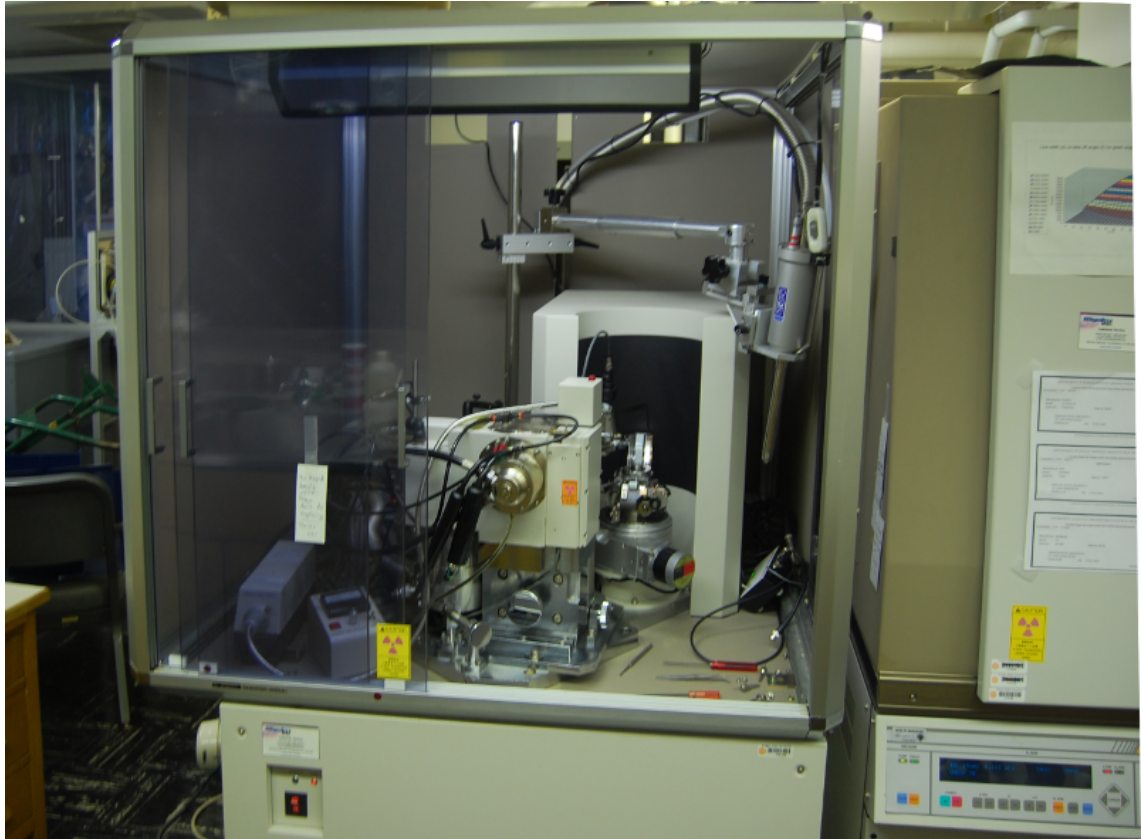


Figure 3.5: Rigaku Rapid X-Ray Diffraction Instrument

$$b_G = \frac{4\ln 2}{H^2}$$

and the Lorentzian function:

$$L(x) = \frac{a_L}{1 + b_L x^2}$$

$$a_L = \frac{2}{\pi H}$$

$$b_L = \frac{4}{H^2}$$

which are mixed using the Pseudo-Voigt function:

$$pV(x) = \eta L'(x) + (1 - \eta)G'(x)$$

These functions were fit to the magnesium oxide, which sets up the instrument correction when performing crystal size measurements.

Fitting a model to experimental data will never achieve a perfect fit. The measurements to determine how well the model fits are the Profile Factor, Weighted Profile Factor, and Expected Weighted Profile Factor.

Profile Factor:

$$R_P = 100 \frac{\sum_{i=1,n} |t_i - y_{o,i}|}{\sum_{i=1,n} y_i}$$

Weighted Profile Factor:

$$R_{wp} = 100 \left[\frac{\sum_{i=1,n} w_i |y_i - y_{o,i}|^2}{\sum_{i=1,n} w_i y_i^2} \right]^{1/2}$$

Expected Weighted Profile Factor:

$$R_{exp} = 100 \left[\frac{n - p}{\sum_i w_i y_i^2} \right]^{1/2}$$

Since the nanoparticle peaks are very weak and broad due to the size effects, resulting in a poor signal to noise ratio, very large residuals were observed. In this system, a R_{exp} value of 50 percent was considered acceptable. This could be lowered by increasing the exposure time in the XRD experiment, however it was impracticable due to time constraints.

3.4.2 Synthesis of Nano Particles via Micromixer

To determine the effects of various variables on the creation of nanoparticles in a micromixer system. A 2^{3-1} factorial experiment was performed to test the effects of the ratio of Fe(III) to NaBH_4 solutions, if the presence of a palladium seeds, and changing the pH of the reactant solution. The flow ratio of the two streams was changed from 1:1 to 1:2 where the latter has a higher rate of the BH_4 solution. Palladium seeds were added at a ratio of 1 palladium ion to 1000 iron ions. For pH adjustment, 0.5 mL of Ammonia was added to the Iron solution. The raw data was analyzed with the help of Statgraphics, which yielded Table 3.6.

The conclusions that can be drawn from this experiment are not very specific. One observation during the experiment was that the effluent of the reactor was still producing gas, which lead to the conclusion that the reaction was not complete

Table 3.6: Synthesis of Nano Particles via Micromixer Design of Experiment 1 Analysis of Variance.

Analysis of Variance					
Source	Sum of Squares	Df	Mean Square	F-Ratio	P-Value
A:Ratio	37.4545	1	37.4545	8.23	0.0641
B:Pd	84.565	1	84.565	18.58	0.023
C:pH	74.481	1	74.481	16.36	0.0272
blocks	2.98901	1	2.98901	0.66	0.4771
Total error	13.6569	3	4.55231		
Total (corr.)	213.146	7			

when it left the reactor. Further particle growth could have been happening in the collection vessel. This can increase the experimental error. The manner in which this experiment is designed also increases the ambiguity of the data. This factorial experiment only has a resolution of three, which means that the main effects are aliased with the first interaction effects. In this case, A is aliased with BC, B is aliased with AC, and C is aliased with AB. In Figure 3.6, the p-value for A is just over the 95 percent confidence interval, therefore it is not considered an important factor. However, at a 90 percent confidence interval, it would be significant. Both factors B and C are significant at the 95 percent confidence interval. It is likely that there is an interaction between these two factors, which would add to the sum of squares to factor A. It is therefore concluded that factor A is not significant.

A second factorial experiment was conducted to further understand how to control the size of nanoparticles created in the micromixer system. This experiment addressed the issue of the delay tube being too short. The first factorial experiment had a 12 inch delay line on the exit of the micromixer. In this experiment, the

Table 3.7: Synthesis of Nano Particles via Micromixer Design of Experiment 2 Analysis of Variance.

Analysis of Variance for Size					
Source	Sum of Squares	Df	Mean Square	F-Ratio	P-Value
A:pH	2.18405	1	2.18405	69.89	0.0758
B:Pd	86.7245	1	86.7245	2775.18	0.0121
C:Reactor Size	0.49005	1	0.49005	15.68	0.1575
AB	28.125	1	28.125	900	0.0212
AC	0.405	1	0.405	12.96	0.1725
BC	0.5202	1	0.5202	16.65	0.153
Total error	0.03125	1	0.03125		
Total (corr.)	118.48	7			

length of the delay line was increased to five feet. There was no evidence of gas formation in the effluent of this reactor configuration, which led to the assumption that the reaction was completed before leaving the delay line. A factor was added to study the effect of the delay tube diameter, which ranged from 0.002 inches to 0.003 inches. The palladium solution (0.01 M) addition was added at a low level of 0.01 mL and a high level of 0.5 mL. The pH was adjusted by the addition of Ammonia (14 N) at a low level of 0.1 mL and a high level of 0.5 mL.

The conclusions that can be drawn in this experiment are much clearer than the previous. This factorial had a resolution of four, no main effect is aliased with another main effect, or a two factor interaction. The diameter of the delay tube did not have a significant effect on the size of the nanoparticles. The concentration of palladium and the interaction of palladium and pH had a significant effect. The palladium ions act as seeds for particle growth, allowing the reaction to skip

the nucleation phase. It is thought that the number of palladium ions in the system will change the total number of particles formed. When maintaining a constant concentration of iron atoms, a change in the number of particles formed will change the number of iron atoms per particle, thus changing the particle size. The interaction with pH modification is thought to come from the formation of a micelle around the palladium ion, which is effected by a change in pH. This causes the particles to grow slower at lower pH, which leads to smaller particles.

3.4.3 SEM Analysis

When the particles are viewed through a microscope the particle size is very different from that shown when examined by x-ray diffraction. The difference between these two measurements are physical particle size, and crystal grain size. In the application the synthesized particles are designed for, the crystal size is more important than the physical particle size. The size of the crystal directly affects the magnetic properties of the material. Freeze dried particles synthesized in a batch reactor can be seen in Figure 3.6. The particles in this figure seem to be large. When the magnification is increased, as in Figure 3.7, the size of the particles start to come through, it appears that the large structure is actually made of smaller particles. At a further increase of magnification, as seen in Figure 3.8, it is clear that the particles are nano-size in scale. The maximum magnification possible on the instrument, Figure 3.9, clearly demonstrates the physical particle size, which ranges from 25 nm to 100 nm. The important aspect from this analysis

is the particles are multi-crystalline. This should not affect the magnetic properties of the material in powder form. A problem may arise when the particles are aligned using an externally applied magnetic field. For future work it is important to be able to align the all particles in along a specific crystallographic direction.

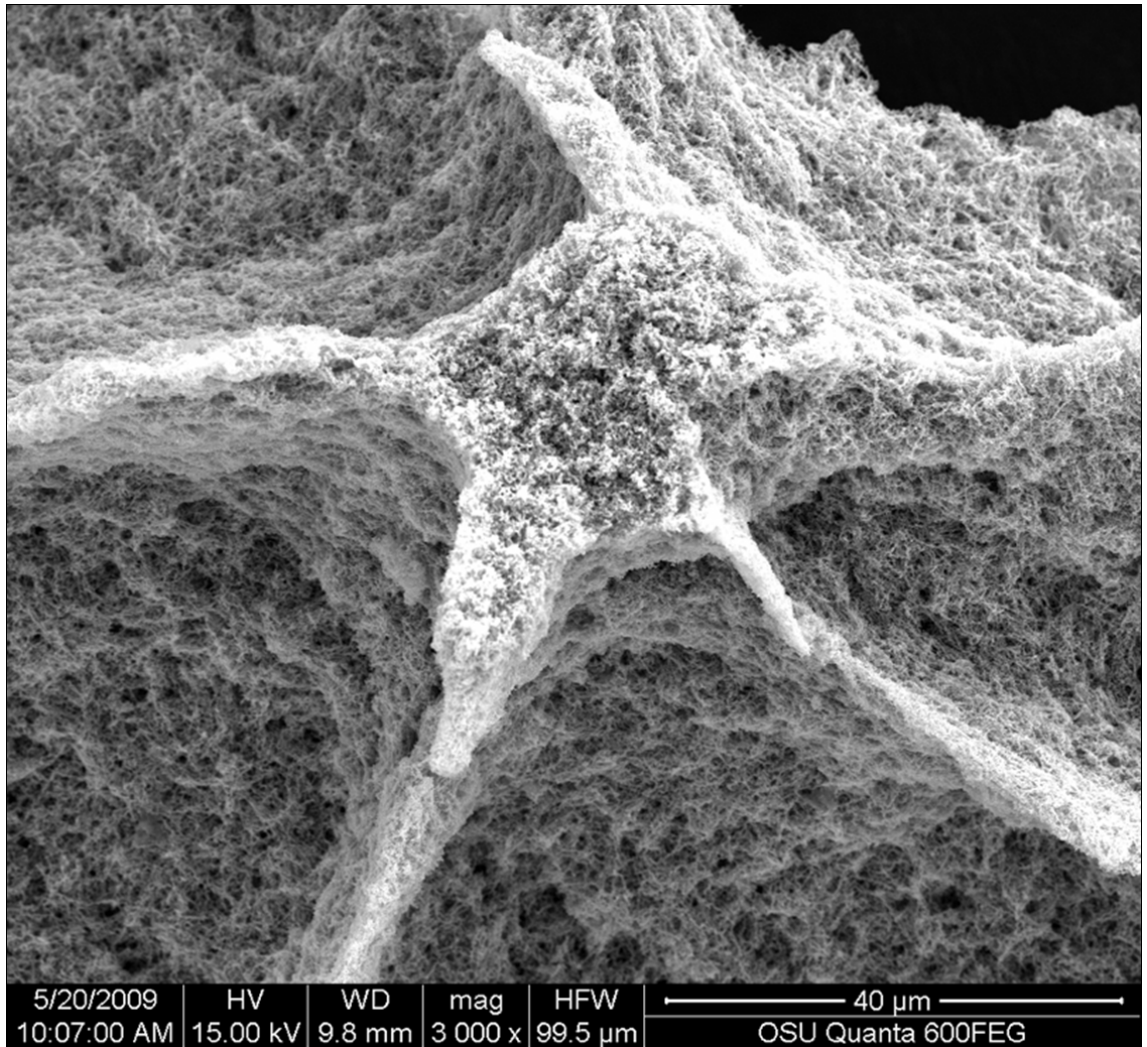


Figure 3.6: SEM image of Iron nano particles at 3000x magnification.

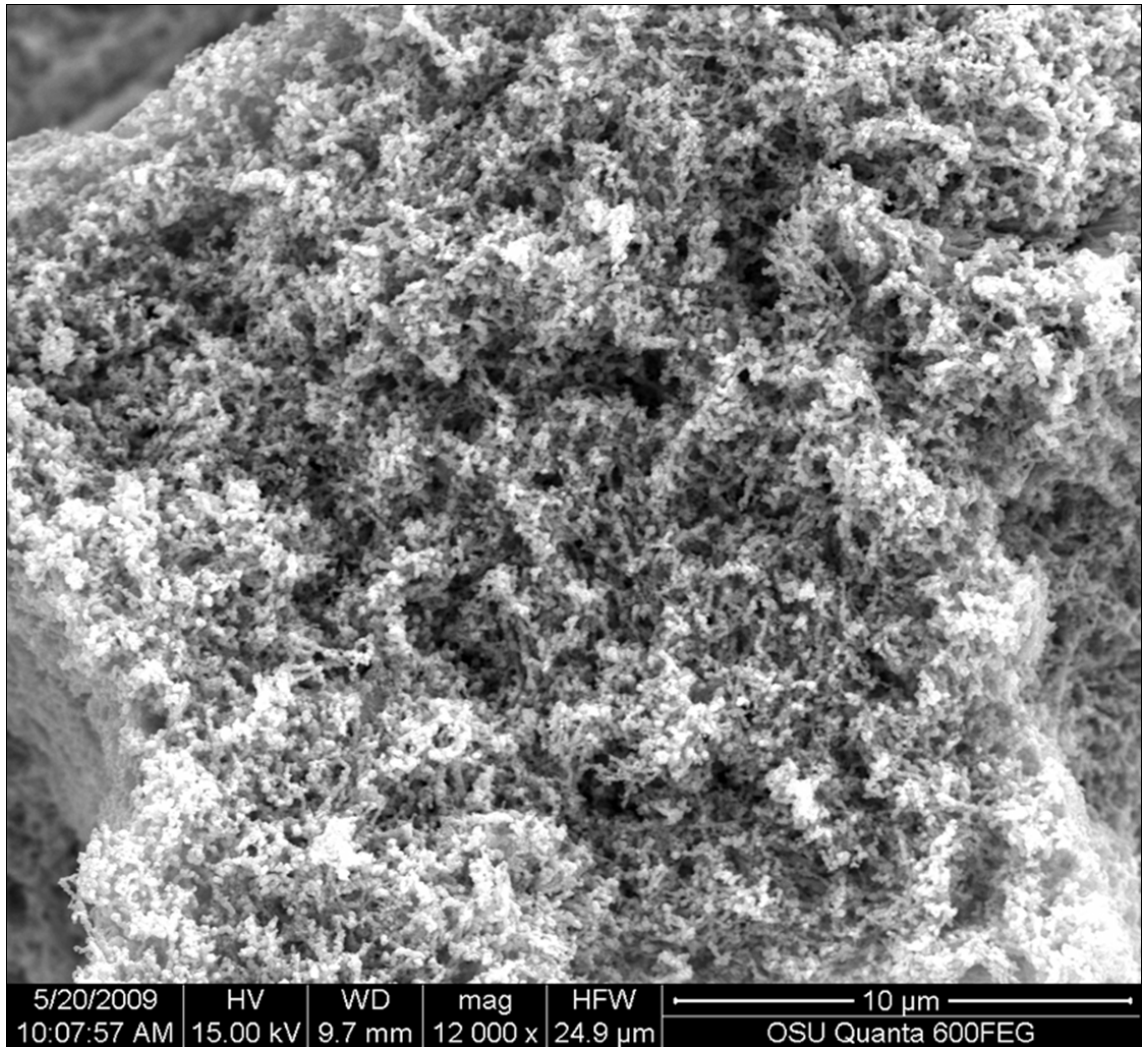


Figure 3.7: SEM image of Iron nano particles at 12,000x magnification.

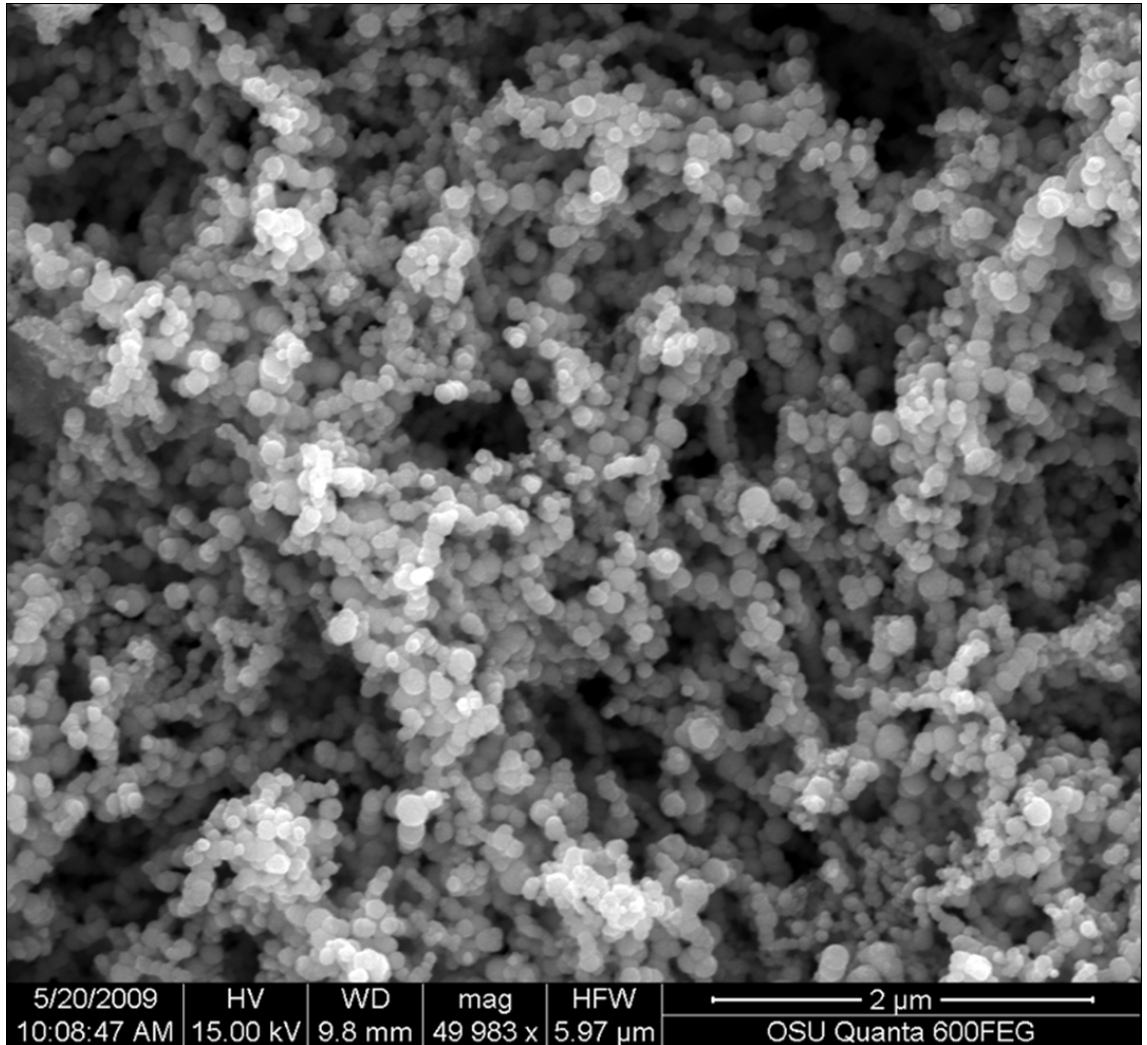


Figure 3.8: SEM image of Iron nano particles at 50,000x magnification.

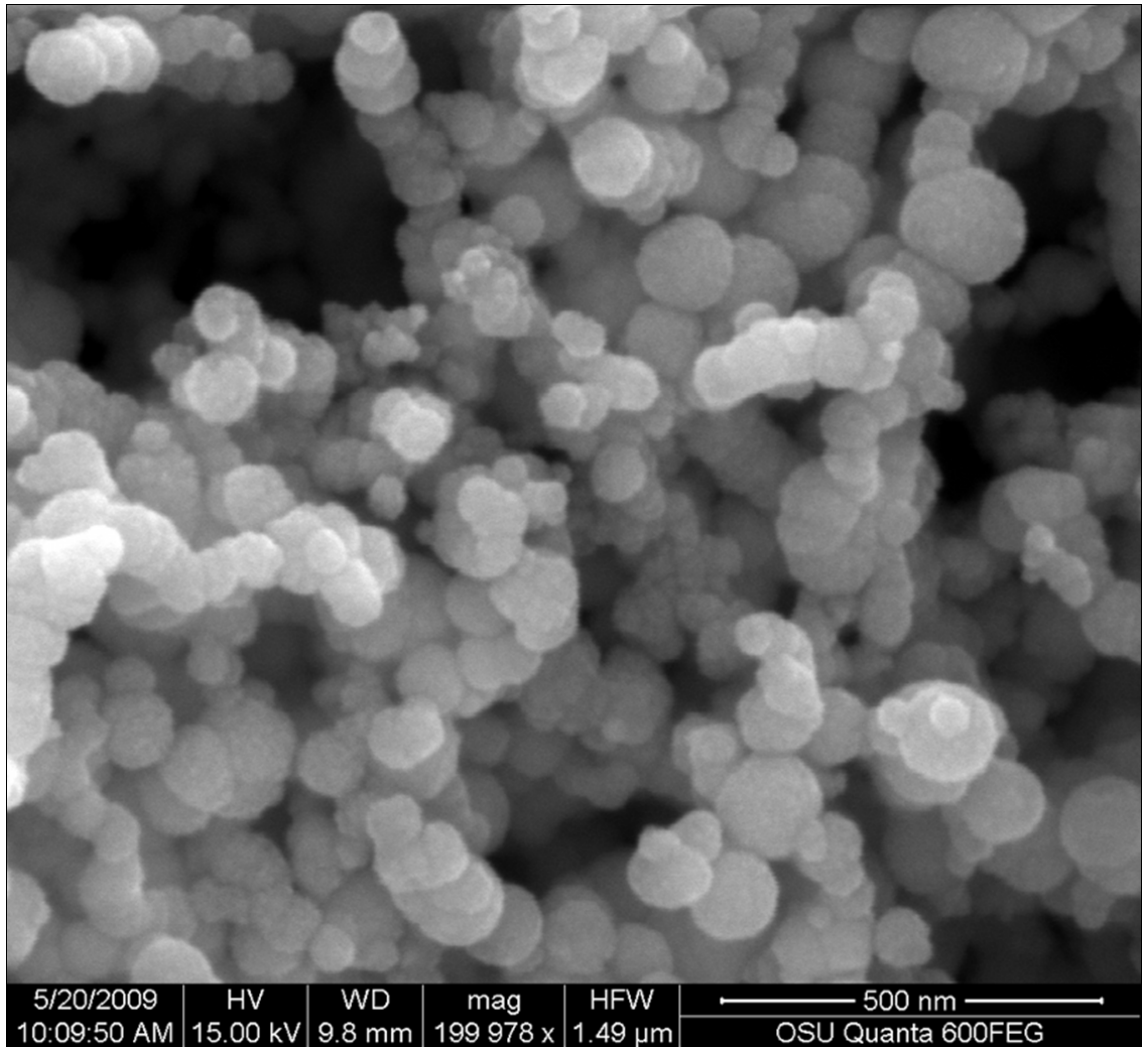


Figure 3.9: SEM image of Iron nano particles at 200,000x magnification.

4. Conclusions and Recommendations

The relative magnetic permeability of an iron epoxy composite material was measured. A measurement device was created to measure the relative magnetic permeability for the specific application. This device proved to be accurate and reliable. The magnetic properties of composite materials has been shown to be controllable, with a linear response to volume fraction of iron in the composite. A maximum relative magnetic permeability was achieved at 650. Curing the composite material in a magnetic field proved to increase the relative magnetic permeability of the composite when the axis that the composite was aligned was the same as the direction that the measurement device reads. The perpendicular direction produced no change in relative magnetic permeability.

Future work in this area should be focused on methods to increase the relative magnetic permeability. These methods include changing the particle size loaded into the material, mixing particle sizes, altering the viscosity of the epoxy, changing the type of binding agent in the composite material away from an epoxy, such as a UV curable material.

A superparamagnetic material is desired for use in high frequency inductors. Iron nanoparticles were explored for use as a superparamagnetic material. Iron nanoparticles were produced in both a batch reactor and a microfluidic system. Iron nanoparticles need to less than 20 nm to be superparamagnetic. The microfluidic system consisted of a micromixer provided by NanoBits, Inc. and five foot length of PEEK tubing. A DOE was performed on the microfluidic system

to determine the important factors when controlling the size of iron nanoparticles, which resulted in the number of palladium seed ions being most important. The nanoparticles were measured for crystal size by XRD using Rietveld refinement to model the size/strain broadening caused by the small crystal size. Rietveld analysis was performed with the help of the software package FullProf. Iron nanoparticles ranging from 1.5 - 10 nm were produced as a result of the microfluidic system.

The following is a list of recommendations for future work:

1. Nanoparticles for use in nano composite testing should be synthesized via batch reactor process. The micromixer was very difficult to work with, due to clogging issues. If the micromixer is used for future work, an alternative reducing agent such as hydrazine should be explored. Hydrazine should be more stable, reducing the amount of gas formed in the pre-reaction section.
2. Optimize process to create single crystalline particles for use in magnetically aligned nano composite. Particle size measurements (SEM, TEM, DLS) in addition to crystal size measurements (XRD) should be performed when performing DOEs. This will allow an interaction between crystal size and particle size to be explored.
3. Magnetic property testing on nanoparticles to test for superparamagnetic properties. B-H loop measurements need to be performed to test if the iron nanoparticles are truly a superparamagnetic material. Other important information such as the relative magnetic permeability can be determined from these measurements.

4. Integration of the nanoparticles into a composite material. Magnetic properties of the composite material need to be tested to determine if the material behaves the same in a composite as in the bulk. The composite should then be cured in a magnetic field and tested for changes in the magnetic properties. The degree of alignment can be determined by XRD.

Bibliography

- [1] K.C. Huang and S.H. Ehrman. Synthesis of Iron Nanoparticles via Chemical Reduction with Palladium Ion Seeds. *Langmuir*, 23(3):1419–1426, 2007.
- [2] D. Vollath. *Nanomaterials: An Introduction to Synthesis, Properties and Applications*. Vch Verlagsgesellschaft Mbh, 2008.
- [3] DH Han, JP Wang, and HL Luo. Crystallite size effect on saturation magnetization of fine ferrimagnetic particles. *Journal of magnetism and magnetic materials*, 136(1-2):176–182, 1994.
- [4] R. Lane, B. Craig, and W. Babcock. Materials engineering with nature’s building blocks. *AMPTIAC Newslett Spring*, 6(1):31–37, 2002.
- [5] L.L. Marzan and P. Kamat. *Nanoscale Materials*. Kluwer Academic Publishers, Massachusetts, USA, 2003.
- [6] H.S. Nalwa. *Handbook of nanostructured materials and nanotechnology*, volume 1. Academic Press, 2000.
- [7] S. Hussain, M. Iqbal, and M. Mazhar. Size control synthesis of starch capped-gold nanoparticles. *Journal of Nanoparticle Research*, pages 1–9, 2009.
- [8] Y. Champion, S. Guérin-Mailly, J.L. Bonnentien, and P. Langlois. Fabrication of bulk nanostructured materials from metallic nanopowders: structure and mechanical behaviour. *Scripta Materialia*, 44(8-9):1609–1613, 2001.
- [9] W. Chang, G. Skandan, SC Danforth, BH Kear, and H. Hahn. Chemical vapor processing and applications for nanostructured ceramic powders and whiskers. *Nanostructured materials*, 4(5):507–520, 1994.
- [10] V.P. Dravid, J.J. Host, MH Teng, B.E.J. Hwang, D.L. Johnson, T.O. Mason, and J.R. Weertman. Controlled-size nanocapsules. 1995.
- [11] PM Ajayan. Nanotubes from carbon. *Chem. Rev*, 99(7):1787–1800, 1999.

- [12] H. Kajiura, H. Huang, S. Tsutsui, Y. Murakami, and M. Miyakoshi. High-purity fibrous carbon deposit on the anode surface in hydrogen DC arc-discharge. *Carbon*, 40(13):2423–2428, 2002.
- [13] CY Wang, WQ Jiqng, Y. Zhou, YN Wang, and ZY Chen. Synthesis of α -Fe ultrafine particles in a saturated salt solution/isopropanol/PVP microemulsion and their structural characterization. *Materials Research Bulletin*, 35(1):53–58, 2000.
- [14] M. Yoshimura and S. Sōmiya. Hydrothermal synthesis of crystallized nanoparticles of rare earth-doped zirconia and hafnia. *Materials Chemistry & Physics*, 61(1):1–8, 1999.
- [15] H. Wang, X. Kou, L. Zhang, and J. Li. Size-controlled synthesis, microstructure and magnetic properties of Ni nanoparticles. *Materials Research Bulletin*, 43(12):3529–3536, 2008.
- [16] S. Sun and H. Zeng. Size-controlled synthesis of magnetite nanoparticles. *Journal of the American Chemical Society*, 124(28):8204–8205, 2002.
- [17] V. Hessel, H. Löwe, and F. Schönfeld. Micromixers a review on passive and active mixing principles. *Chemical Engineering Science*, 60(8-9):2479–2501, 2005.
- [18] N.T. Nguyen and Z. Wu. Micromixers a review. *J. Micromech. Microeng*, 15(2):R1–R16, 2005.
- [19] J. Wagner, T. Kirner, G. Mayer, J. Albert, and JM Köhler. Generation of metal nanoparticles in a microchannel reactor. *Chemical Engineering Journal*, 101(1-3):251–260, 2004.
- [20] HM Rietveld. A profile refinement method for nuclear and magnetic structures. *Journal of Applied Crystallography*, 2(2):65–71, 1969.
- [21] J. Rodriguez-Carvajal. Recent advances in magnetic structure determination by neutron powder diffraction. *Physica. B, Condensed matter*, 192(1-2):55–69, 1993.
- [22] R.A. Young. *The Rietveld Method*. Oxford University Press, USA, 1995.

- [23] JJ Olivero and RL Longbothum. Empirical fits to the Voigt line width: a brief review. *Journal of Quantitative Spectroscopy and Radiative Transfer*, 17(2):233–236, 1977.
- [24] G. Caglioti, A. Paoletti, and FP Ricci. Choice of collimators for a crystal spectrometer for neutron diffraction. *Name: Nuclear Instr*, 1958.
- [25] L. Lutterotti and P. Scardi. Simultaneous structure and size-strain refinement by the Rietveld method. *Journal of Applied Crystallography*, 23(4):246–252, 1990.
- [26] M. Leoni, R. Maggio, S. Polizzi, and P. Scardi. X-ray diffraction methodology for the microstructural analysis of nanocrystalline powders: Application to cerium oxide. *Journal of the American Ceramic Society*, 87(6):1133–1140, 2004.
- [27] R.A. Fisher. *The Design of Experiments*. Macmillan Pub Co, 1971.
- [28] D.C. Montgomery. *Design and Analysis of Experiments*. John Wiley & Sons, 6th edition, 2005.

